Biosensors and Bioelectronics 180 (2021) 113114

Contents lists available at ScienceDirect

Biosensors and Bioelectronics

journal homepage: http://www.elsevier.com/locate/bios

An ultrasensitive heart-failure BNP biosensor using B/N co-doped graphene oxide gel FET

I. Novodchuk [a,b,*], M. Kayaharman [c,b], I.R. Ausri [d,b], R. Karimi [e], X.S. Tang [d,b], I. A. Goldthorpe [c,b], E. Abdel-Rahman [f], J. Sanderson [e], M. Bajcsy [c,g], M. Yavuz [a,b]

[a] Mechanical and Mechatronics Engineering, University of Waterloo, Waterloo, ON, Canada
[b] Waterloo Institute for Nanotechnology (WIN), University of Waterloo, Waterloo, ON, Canada
[c] Department of Electrical and Computer Engineering, University of Waterloo, Waterloo, ON, Canada
[d] Department of Chemistry, University of Waterloo, Waterloo, ON, Canada
[e] Dept. of Physics and Astronomy, University of Waterloo, Waterloo, ON, Canada
[f] Dept. of Systems Design Engineering, University of Waterloo, Waterloo, ON, Canada
[g] Institute for Quantum Computing, University of Waterloo, Waterloo, ON, Canada

ARTICLE INFO

Keywords:
FET
Biosensor
Graphene-based
Heart failure

ABSTRACT

Heart failure (HF) is the number one cause of death in the world. B-type natriuretic peptide (BNP) is a recognized biomarker for HF and can be used for early detection. Field effect transistor (FET) biosensors have the ability to sense BNP in much shorter times than conventional clinical studies. The lowest limit of detection (LOD) of state-of-the-art HF FET biosensors is 100 fM and detection ranges are short, being less than 4 orders of magnitude. In this work, a B/N co-doped graphene oxide (GO) gel (BN-GO) was used as the channel material in an FET biosensor targeting BNP. The sensor was able to sense BNP in as little as 2 min, with an LOD as low as 10 aM and a wide linear detection range of 10 aM–1 μM, stretching over 11 orders of magnitude. The biosensor showed great selectivity and minimal response towards K^+ and OH^- ions and the human epidermal growth factor receptor (HER2) protein. This biosensor serves as a proof-of-concept of the ability of BN-GO gel FETs to be used for ultrasensitive biosensors.

1. Introduction

Heart failure (HF) currently affects 26 million people worldwide (Ferreira et al., 2019) and is the most prevalent cause of death in the world (Alawieh et al., 2019). Early diagnosis of HF is vital to improve prognosis, but current protocols are time consuming. Thus, there is a dire need for a sensitive and faster biosensing platforms to detect HF biomarkers, such as B-type natriuretic peptide (BNP) (Li et al., 2019). In recent years, many researchers have studied field effect transistors (FETs) as a platform for different biosensing applications ranging from cancer (Mu et al., 2015) to viruses (Seo et al., 2020) or bacteria (Moudgil et al., 2020). These applications are especially attractive for their point-of-care applications, sensitivity, fast detection capability, and compatibility with complementary metal-oxide-semiconductor (CMOS) fabrication. Lately, graphene-based field effect transistors (GFETs) have emerged as attractive biosensors for ultrasensitive detection thanks to the theoretical extremely-high charge carrier mobility of graphene which reaches 200,000 $cm^2\ V^{-1}s^{-1}$ (Novodchuk et al., 2020). It was demonstrated that the charge carrier mobility of GFET has a direct affect over its sensitivity and limit of detection (LOD). Nonetheless, very few works have demonstrated the ability to fabricate GFETs biosensors exceeding a charge carrier mobility of 1000 $cm^2\ V^{-1}s^{-1}$ at room temperature.

While pristine graphene FETs lack the required charge carrier mobility, composites of B, N and graphene have been shown to exhibit high charge carrier mobilities. Hybrid structures of graphene and BN were shown to have a mobility of ~36,000 $cm^2\ V^{-1}s^{-1}$ (Stolyarov et al., 2015). B/N co-doped graphene oxide (GO) gels were shown to have a mobility of 9000 $cm^2\ V^{-1}s^{-1}$ (Novodchuk et al., 2019b), (Novodchuk et al., 2019a). And other works (Su, Y., Cao, S., Shi, L. B., & Qian, 2020) have shown that the mobility of B/N/C materials can reach ~100,000 $cm^2\ V^{-1}s^{-1}$.

Debye screening (Piccinini et al., 2018) is another limiting factor in GFET biosensors since its length is below 1 nm in physiological solutions

* Corresponding author. 200 University Ave W, Waterloo, ON, N2L 3G1, Canada.
E-mail address: inovodch@uwaterloo.ca (I. Novodchuk).

https://doi.org/10.1016/j.bios.2021.113114
Received 22 December 2020; Received in revised form 8 February 2021; Accepted 20 February 2021
Available online 26 February 2021

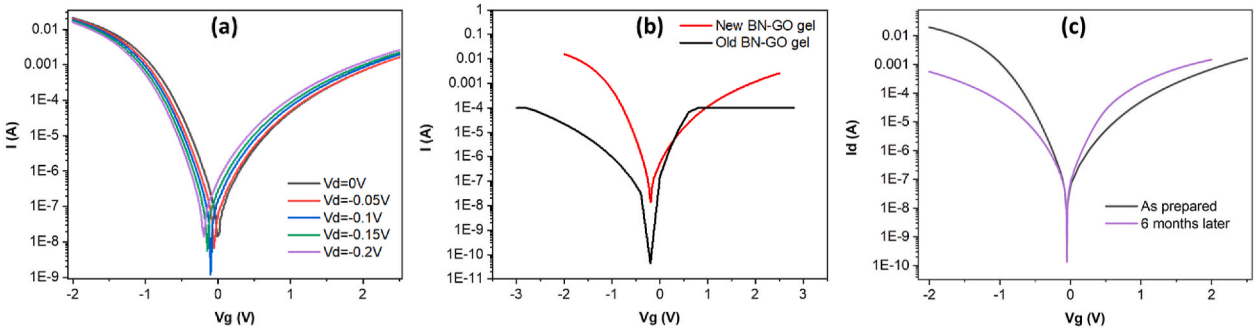

Fig. 1. The electrical properties of the BN-GO FET devices. (a) Drain current vs gate voltage for increasing drain voltages. (b) A comparison between the electrical performance of gels used in this work with those previously reported (for a drain voltage of −0.1 V) (Novodchuk et al., 2019b). (c) The electrical performance over time (for a drain voltage of −50 mV).

(Gao et al., 2016), while the typical size of a bioreceptor exceeds this length. Lately, researchers were able to overcome this obstacle by either using compressed graphene or using concave structures which were shown to effectively increase the Debye screening length (Hwang et al., 2020).

In this work, a B/N co-doped GO (BN-GO) gel was used for the first time as the channel material in a back-gated FET biosensor. The device was tested as a proof-of-concept towards its detection ability of BNP. To achieve detection, the device was functionalized with a BNP antibody (50E1 antibody) without the use of a linker, due to the presence of ammine and carboxyl groups in the BN-GO gel (Novodchuk et al., 2019b), (Martin, 1998). The biosensor exhibits an extremely low LOD of 10 aM and a large detection range which stretches over 11 orders of magnitude (10 aM-1 μM) in buffer solution. This sensitivity is attributed to its extremely high mobility and non-flat morphology. The detection time is as little as 2 min.

2. Experimental

2.1. Fabrication of BN-GO FETs

BN-GO gel FETs were fabricated in the same process as previously reported (Novodchuk et al., 2019b), (Mistry et al., 2020). In short, femtosecond laser ablation was used to fabricate the BN-GO gel from a BN quantum dot and GO solution by using pulses from a 1 kHz 35 fs laser with an average power of 1 W focused by a 5 cm lens, 2 mm below the surface of the solution for 50 min while constantly stirring using a magnetic stirrer. The gel was spin-coated between pre-patterned Au/Ti source and drain electrodes on a SiO_2/p-Si substrate. The x-ray photoelectron spectroscopy (XPS) analysis, the schematic structure of the BN-GO gel, and the scanning electron microscope (SEM) images of the curved gel surface could be seen in Figs. S1–S3 in the Supporting Information, respectively.

2.2. Antibody immobilization

A pH = 7 buffer solution (Thermo Scientific) was used in all biosensing experiments. BNP antibodies (50E1) were diluted in buffer to a 1 nM solution. 5 μL droplets were dropped onto the BN-GO channels and left at 4 °C for 48 h. The antibodies attached to the carboxyl groups in the channels (Welch et al., 2017). It is well established that carboxyl groups can be used for direct immobilization, as discussed in (Filippidou et al., 2019). From the XPS analysis (Fig. S1 in the Supporting Information), the concentration of carboxyl groups in the gel is 9.9 at%. The process for bioreceptor immobilization followed the recipe discussed in (Ju et al., 2015). The immobilization of the antibodies was confirmed by the shift of the Dirac point, similar to observations made elsewhere (Lei et al., 2017). To confirm a strong immobilization of antibodies, the device went through three consecutive rinsing rounds. In each rinsing round, 10 μL droplets of buffer solution were pipetted on and off the device 5 times.

2.3. Immunodetection

All electrical measurements were performed using a probe station setup connected to a software-controlled source measure unit (KEYSIGHT B2900A Series). The BNP biomarker was serially diluted to multiple concentrations in buffer solution. For the real-time measurements, a 2.5 μL BNP solution with increasing concentrations was dropped onto the BN-GO gel channel every 50 s, approximately, while continuously monitoring the device's current (for constant drain and back gate voltages of −0.05 V and −0.6 V, respectively). For the Dirac point change monitoring, 2.5 μL of BNP solution with increasing concentrations was dropped onto the channel, and a drain current vs gate voltage plot was obtained after 2 min (at a constant drain voltage of −0.05 V). Then the channel was rinsed with buffer solution and the measurement was repeated with a higher concentration of BNP. The results for buffer solution were taken as the reference for both measurements. Specificity experiments were performed in the same manner described above, but for unfunctionalized BN-GO gel FET devices. Selectivity experiments were monitored in two ways. First, the device's current was continuously monitored for constant gate and drain voltages (of −1.5 V and −50 mV, respectively). Different concentrations of K^+ and OH^- solution in a pH = 7 buffer were pipetted onto the channel and the change in current was monitored. Second, the change in the Dirac point of the BNP biosensor was monitored in the same way described above, but instead of adding BNP solution, different concentrations of human epidermal growth factor receptor (HER2) in pH = 7 buffer were pipetted onto the channel. The ELISA test for 50E1 and BNP confirming the immunoassay was previously reported (Li et al., 2019).

3. Results and discussion

3.1. Electrical properties

GFETs could be used as biosensors when they are functionalized with a bioreceptor that would specifically bind to the desired biomarker (Novodchuk et al., 2020). The biosensing could be achieved by either monitoring the change in their current versus time for constant applied biases or by monitoring the change in the Dirac point as a direct result from the attachment of a charged biomarker to the bioreceptor. Since the biomarker is charged, it will induce a change in the number of charges in the semiconductor transducer, translating to a current and Dirac point change, respectively. For a p-type channel, a negatively charged biomarker would increase the current and shift the Dirac point to the left.

The back-gated BN-GO gel FETs were fabricated in the same manner as previously reported (Novodchuk et al., 2019b). The electrical

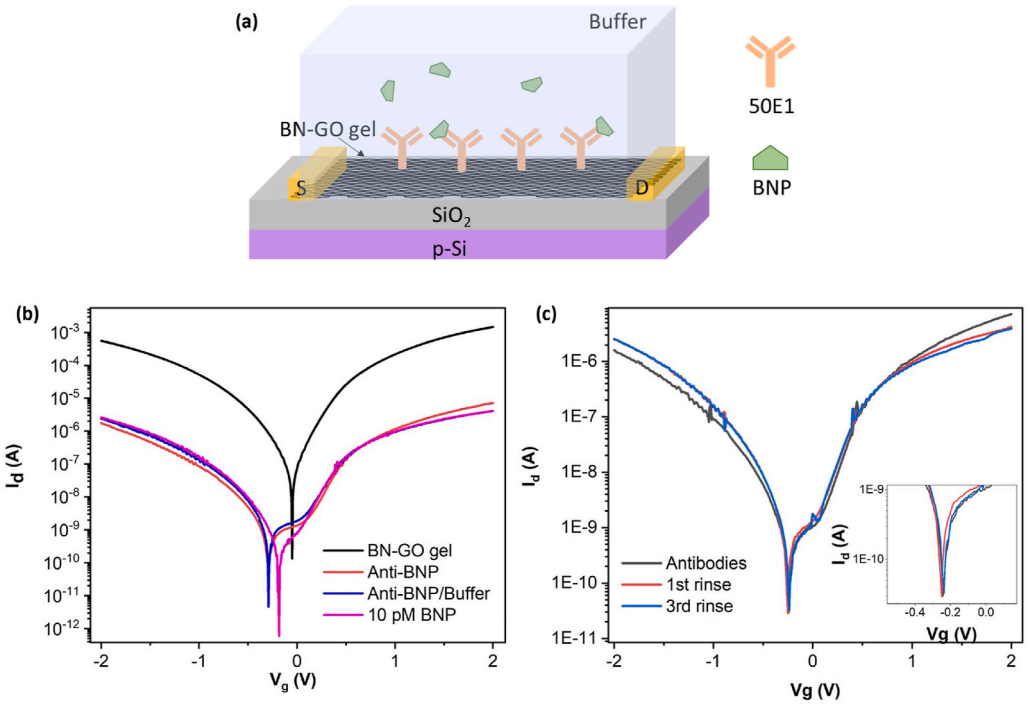

Fig. 2. (a) The device schematics and the biosensing principle. The change in drain current vs gate voltage plot (b) of the BN-GO FET after anti-BNP immobilization and the addition of buffer and 10 pM BNP, and (c) of anti-BNP functionalized BN-GO FET after the first and third rounds of continuous rinsing. The inset of (c) is an enlargement of the Dirac points.

performance of the non-functionalized devices is presented in Fig. 1a. As seen from the drain current versus gate voltage (I_d-V_g) plot, the Dirac point for $V_g = 0$ V is slightly below 0 V, meaning that the device has a slightly more dominant p-type doping (Novodchuk et al., 2020). Since the gels were fabricated in the same mechanism previously reported (old BN-GO gel) (Novodchuk et al., 2019b), the electrical performance of the two gels was compared in Fig. 1b, with the newly fabricated gel denoted as "new BN-GO gel". As seen from the figure, the ON and OFF currents (I_{ON} and I_{OFF}, respectively) increased for the "new" gel with a new I_{ON}/I_{OFF} value of $\sim 10^7$, an order of magnitude larger that the "old" gel. In addition, the charge carrier mobilities were calculated as 440,000 ± 200,000 $cm^2\ V^{-1}s^{-1}$ and 8700 $cm^2\ V^{-1}s^{-1}$ for holes and electrons, respectively. This observation was a great increase from the values observed for the "old" gel of 5000 ± 2500 $cm^2\ V^{-1}s^{-1}$ and 8700 ± 3000 $cm^2\ V^{-1}s^{-1}$ for holes and electrons, respectively. The difference in electrical properties could be a result from the decrease in the laser pulse duration (by a factor of three) used in the fabrication of the "new" gels (Hamad, 2016). The reduced pulse duration translates to increased laser intensity, which in turn can be used to break more bonds in the precursor materials (Roberts, A. et al., 2011), (Ramadhan, A. et al., 2017). An XPS analysis of the gel (Fig. S1 in the Supporting Information) revealed a higher C–C bond concentration (43.6 at%) compared to the "old gel" (41.8 at%) (Novodchuk et al., 2019b). The increased conjugation is expected to be the main reason for the improved charge carrier mobility (Gao et al., 2009).

The stability of the gels was also studied over a period of 6 months, as seen in Fig. 1c. In that time frame, a significant decrease in the hole mobility was observed and a 2-fold reduction in the I_{ON}/I_{OFF} ratio. The charge carrier mobilities of the BN-GO gel after a 6-month storage was calculated as 8800 ± 3500 $cm^2\ V^{-1}s^{-1}$ and 10,000 ± 2500 $cm^2\ V^{-1}s^{-1}$ for holes and electrons, respectively. These were the gels used for the biosensing experiments in this paper.

3.2. Antibody immobilization

Antibody immobilization is one important aspect of the success of a biosensor, since it defines its ability to selectively capture the biotarget from a complex environment (Morales and Halpern, 2018). However, antibodies are large molecules commonly attached to the bioreceptor through linker molecules (Novodchuk et al., 2020) which themselves add approximately 2 nm to the overall bioreceptor length (Kwong Hong Tsang et al., 2019). Considering the length of the Debye layer screening in physiological solutions is below 1 nm (Novodchuk et al., 2020), increasing the antibody length is unfavorable. The BN-GO gels used in this paper were shown to possess pyrrolic N groups, which are categorized as secondary amine groups (Novodchuk et al., 2019b), (Šindler-Kulyk, M., Tomšić, S., Marinić, Ž., & Metelko, 1995). These groups as well as carboxyl groups can be used for covalently immobilizing antibodies (Martin, 1998), (Georgakilas et al., 2012). The antibodies would be used to capture the BNP, as schematically presented in Fig. 2a.

In this paper, the BN-GO channels were incubated in a 50E1 (anti-BNP) solution for 48 h at 4 °C. The immobilization of the anti-BNP was monitored by the change in the drain current versus gate voltage plot, as demonstrated in Fig. 2b. Several changes to the I_d-V_g plot are worth exploring. First, the Dirac point shifted by approximately −30 mV, confirming that the antibodies (pI = 6.6–7.2) are negatively charged. This observation is in line with previous reports (Lei et al., 2017). Second, a large change in the ON and OFF currents was observed after immobilization of antibodies, suggesting the attachment was through covalent bonds, since this type of attachment tends to scatter charges and decrease the current of GFETs (Fu et al., 2017). Lastly, an additional minima point appeared at $V_g \sim 0$ V, further confirming the attachment of the charged antibodies (Kwong Hong Tsang et al., 2019), (Feng et al., 2014). The addition of buffer solution to the antibody-functionalized channels revealed minimal change in the I_d-V_g plot, as seen in the figure. Similarly, the buffer had negligible effect over the I_d-V_g characteristics of the bare BN-GO gel, as seen in Fig. S4 in the Supporting Information.

To further confirm the antibody immobilization was through covalent bonds, the device was subjected to three consecutive rinsing cycles. When antibodies are attached through physical bonds, they can be easily

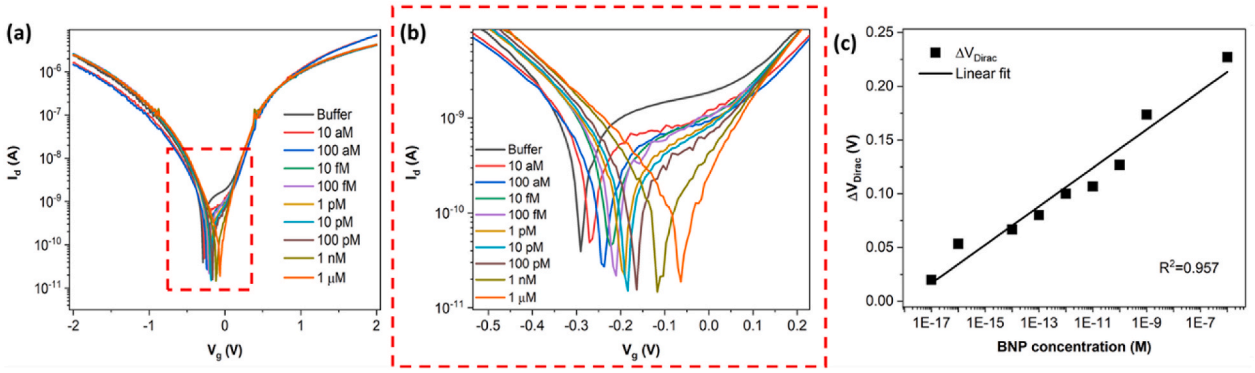

Fig. 3. BNP sensing sensitivity. (a) and (b) the change in drain current vs gate voltage plot in response to increasing concentrations of BNP. (c) The detection range as seen from the Dirac point shift in response to increasing concentrations of BNP.

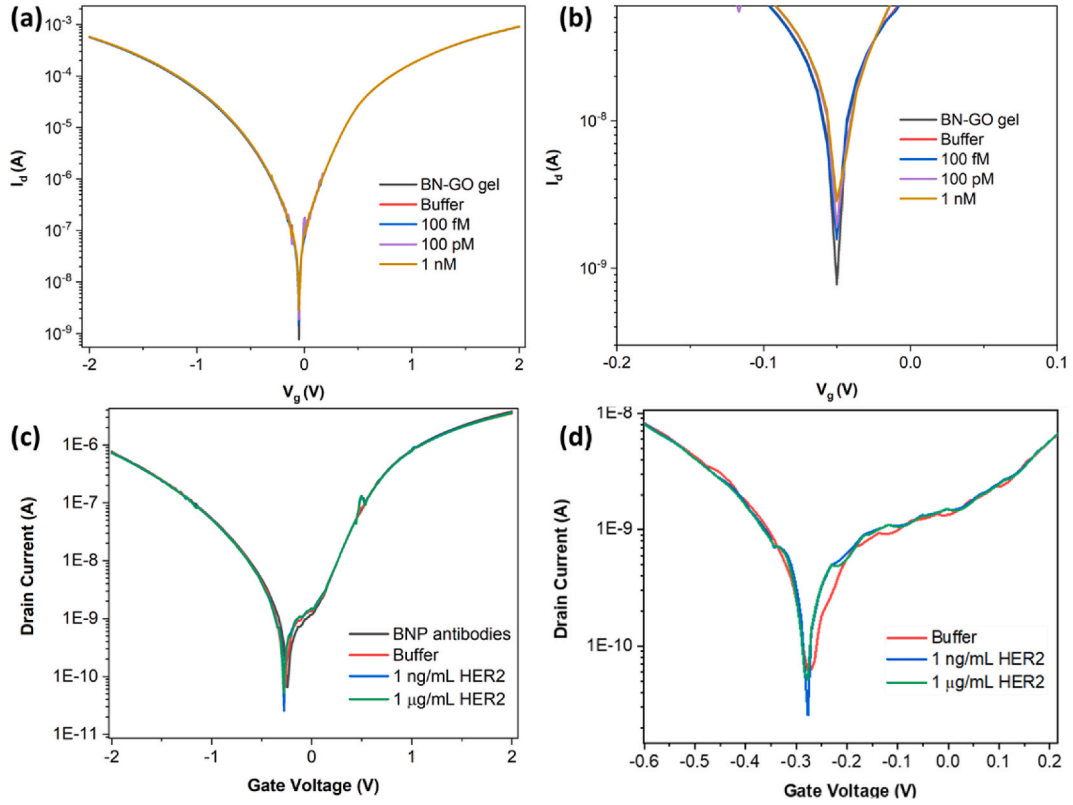

Fig. 4. (a) Specificity and (c) selectivity of the BN-GO gel FET biosensor as seen from the drain current vs gate voltage curves. (b) and (d) are enlarged view of the Dirac points in (a) and (c), respectively.

detached by rinsing the device in buffer (Fu, H., & Liu, 2019). The minimal change in the I_d-V_g characteristics following one and three rinsing cycles presented in Fig. 2c confirms the covalent binding of the antibodies to the BN-GO gel.

3.3. Sensitivity of BNP detection

The sensing mechanism used in this work was achieved through monitoring the Dirac point change in response to the formation of the BNP complex with its antibodies on the BN-GO FET surface (Novodchuk et al., 2020). Since the BNP biomolecules are positively charged (pI = 10.95), the Dirac point is expected to increase (Li et al., 2019). The I_d-V_g were plotted for anti-BNP functionalized BN-GO FET after 2 min incubation in various concentrations of BNP in a pH = 7 buffer, as seen in Fig. 3a–b. The incubation in pure buffer served as the control. As expected, the Dirac point shift towards higher voltages in response to the addition of BNP. Furthermore, the shift increased with increased BNP concentration, with a limit of detection of 10 aM. In addition, the change in the Dirac voltage (ΔV_{Dirac}) plotted against the BNP concentration (C_{BNP}) presented in Fig. 3c exhibited a linear behavior ($R^2 = 0.96$) over the large range of concentrations with the calculated relationship of $\Delta V_{Dirac} = 0.0178 Log C_{BNP} + 0.321$. The figure demonstrates an incredible detection range that stretches over 11 orders of magnitude (10 aM–1 μM). The improved LOD is suspected to stem from two main reasons. First, the increased charge carrier mobility of the FET (Novodchuk et al., 2020), and second, the increased Debye length as a result of curved surfaces in the BN-GO gel (Novodchuk et al., 2019b) as seen in Fig. S3 in the Supporting Information. The effect of curved surfaces on the Debye screening length has been studied elsewhere (Hwang et al., 2020).

Table 1
A summary of the FET BNP biosensing platforms in the state-of-the-art.

Biotransducer	Bioreceptor	Target	LOD	Range	Detection time (min)	Medium	Reference
AlGaN/GaN	Aptamer	NT-proBNP	0.832 pg/mL	50–10,000 pg/mL	5	Human sample	Sinha et al. (2019)
AlGaN/GaN	Aptamer and antibody	NT-proBNP	181 pg/mL	200–5000 pg/mL	5	Serum	Sarangadharan et al. (2017)
Reduced GO/Pt nanoparticles	Antibody	BNP	0.1 pM 50×10^3 pM	100 fM-1 nM 50–200 nM	30 30	Buffer Blood	Lei et al. (2017)
Polyaniline	Antibody	BNP	50 pg/mL (~14 pM) ~129 pg/mL	50–200 pg/mL ~130–300 pg/mL	1 –	Buffer Serum	Liu et al. (2016)
MOSFET	Antibody	NT-proBNP	~100 pg/mL	–	5	Blood	Sarangadharan et al. (2019)
Reduced GO	Antibody	NT-proBNP	10 pg/mL 10^4 pg/mL	10–1000 pg/mL –	15 –	Buffer Serum	Munief et al. (2019)
MOSFET	Antibody	BNP	100 pg/mL (~30 pM) 140 pg/mL	100–500 pg/mL 500–4000 pg/mL	5 5	Buffer Blood	Sarangadharan et al. (2018)
BN-GO gel	Antibody	BNP	10^{-5} pM	10 aM-1 μM	2	Buffer	This work

3.4. Specificity

Specificity of the BN-GO gel FET biosensors were measured by monitoring the Dirac point change in response to increasing BNP concentrations without the immobilization of anti-BNP onto the channel. This experiment was performed to make sure that the BNP is affecting the electrical change in the channel only through connecting to the antibodies, and not through direct immobilization to the gel channel (Li et al., 2019). BNP is a small positively charged molecule; were it to attach to the BN-GO channel, the expected effect would have been an increase in the Dirac point. The experimental results are presented in Fig. 4a–b. As seen in the figures, the Dirac point does not shift when the BNP is introduced to the channel, even at a high concentration of 1 nM. In addition, the BNP has no effect over the charge carrier mobility of the device, unlike when antibodies are attached to the channel.

3.5. Selectivity

The selectivity of the BNP biosensor was measured against HER2, a protein that is over expressed in different types of cancer including breast cancer (Novodchuk et al., 2020). As seen in Fig. 4c–d, the Dirac point slightly shifted when the HER2 was introduced from −0.274 V to −0.277 V, but this 3 mV shift is within the noise of the device, and approximately 10 times lower than the shift for 10 aM BNP. In addition, no further shift was observed for a HER2 concentration of up to 1 μg/mL, which is much higher than the normal range in the blood (12.2 ng/mL) (Asgeirsson et al., 2007).

Selectivity towards other interfering species was also performed, as seen in Fig. S7a in the Supporting Information. The BNP biosensor was continuously monitored when increasing concentrations of K^+ OH^- ions were introduced to the channel. The change in current was up to 3 nA which is within the device's noise. The sensitivity of the sensor was compared in Fig. S7b in the Supporting Information. It is clear from the figure that the devices sensitivity is much more pronounced to BNP compared to HER2 and K^+ OH^- ions, confirming the selectivity of the device.

3.6. State-of-the-art

The BNP biosensor was compared to similar FET biosensors reported in recent years, as seen in Table 1. The transducer, bioreceptor, target, and biosensing capabilities were compared. The BNP biosensor used in this work exhibits both superior LOD and detection range compared to the recent literature. It also exhibits shorter detection times compared to the state-of-the-art with a single exception (Liu et al., 2016). It is important however to note, that this device is only aimed as a proof of concept, and future works should target BNP in more complex samples.

4. Conclusions

In conclusion, the ability to fabricate a BNP biosensor using a BN-GO gel FET covalently functionalized with BNP antibodies was demonstrated. The biosensor was able to detect BNP in buffer with an LOD as little as 10 aM within 2 min. The superior detection range achieved by the biosensor stretched over 11 orders of magnitude (10 aM–1 μM). In addition, the biosensor had minimal response towards interfering species and minimal non-specific reactions. These results show the potential towards point-of-care applications of HF monitoring using BN-GO gel FET biosensors. Future experiments should target BNP detection in more complex metrices, such as blood or serum.

Data availability

The raw/processed data required to reproduce these findings cannot be shared at this time due to technical or time limitations.

CRediT authorship contribution statement

I. Novodchuk: Conceptualization, Methodology, Data curation, Writing – original draft. **M. Kayaharman:** Conceptualization, Data curation. **I.R. Ausri:** Resources, Writing – review & editing. **R. Karimi:** Resources. **X.S. Tang:** Resources, Writing – review & editing. **I.A. Goldthorpe:** Resources, Writing – review & editing. **E. Abdel-Rahman:** Resources, Writing – review & editing. **J. Sanderson:** Resources, Writing – review & editing. **M. Bajcsy:** Supervision, Resources, Writing – review & editing. **M. Yavuz:** Supervision, Resources, Writing – review & editing.

Declaration of competing interest

The authors declare that they have no known competing financial interests or personal relationships that could have appeared to influence the work reported in this paper.

Acknowledgements

The authors gratefully acknowledge financial support by the Ontario Graduate Scholarship (OGS) and NSERC-Discovery programs, and the

Ontario Ministry of Research and Innovation Early Researcher Award. The authors would like to thank Dr. Monika Snowden for her chemical expertise and advice.

Appendix A. Supplementary data

Supplementary data to this article can be found online at https://doi.org/10.1016/j.bios.2021.113114.

References

Alawieh, H., Chemaly, T. El, Alam, S., Khraiche, M., 2019. Sensors 19, 1–25.
Asgeirsson, K.S., Agrawal, A., Allen, C., Hitch, A., Ellis, I.O., Chapman, C., et al., 2007. Breast Cancer Res. 9 (6), R75.
Feng, T., Xie, D., Wang, D., Wen, L., Wu, M., 2014. J. Appl. Phys. 116.
Ferreira, J.P., Kraus, S., Mitchell, S., Perel, P., Piñeiro, D., Chioncel, O., Colque, R., de Boer, R., Gomez-Mesa, J.E., Grancelli, H., Lam, C.S., 2019. Glob. Heart 14 (3), 197–214.
Filippidou, M.K., Loukas, C.M., Kaprou, G., Tegou, E., Petrou, P., Kakabakos, S., Tserepi, A., Chatzandroulis, S., 2019. Microelectron. Eng. 216, 111093.
Fu, H., Liu, X., 2019. J. Micromech. Microeng. 29 (12), 124003.
Fu, W., Jiang, L., van Geest, E.P., Lima, L.M.C., Schneider, G.F., 2017. Adv. Mater. 29, 1–25.
Gao, N., Gao, T., Yang, X., Dai, X., Zhou, W., Zhang, A., Lieber, C.M., 2016. Proc. Natl. Acad. Sci. U.S.A. 113, 14633–14638.
Gao, W., Alemany, L.B., Ci, L., Ajayan, P.M., 2009. Nat. Chem. 1, 403–408.
Georgakilas, V., Otyepka, M., Bourlinos, A.B., Chandra, V., Kim, N., Kemp, K.C., Hobza, P., Zboril, R., Kim, K.S., 2012. Chem. Rev. 112 (11), 6156–6214.
Hamad, A.H., 2016. High Energy Short Pulse Lasers, pp. 305–325.
Hwang, M.T., Heiranian, M., Kim, Y., You, S., Leem, J., Taqieddin, A., Faramarzi, V., Jing, Y., Park, I., van der Zande, A.M., Nam, S., Aluru, N.R., Bashir, R., 2020. Nat. Commun. 11, 1543.
Ju, C., Fan, Q., Jia, Y., 2015. A novel biomedical sensor for tumor marker based on Flexible supported solution gated graphene field effective transistor. In: International Conference on Materials. Environmental and Biological Engineering, pp. 429–432. MEBE 2015.
Kwong Hong Tsang, D., Lieberthal, T.J., Watts, C., Dunlop, I.E., Ramadan, S., del Rio Hernandez, A.E., Klein, N., 2019. Sci. Rep. 9, 2–11.
Lei, Y.M., Xiao, M.M., Li, Y.T., Xu, L., Zhang, H., Zhang, Z.Y., Zhang, G.J., 2017. Biosens. Bioelectron. 91, 1–7.
Li, Z., Ausri, I.R., Zilberman, Y., Tang, X.S., 2019. Nanoscale 11, 18347–18357.
Liu, P., Huang, J., Sanchez, D.V.P., Schwartzman, D., Lee, S.H., Yun, M., 2016. Sensor. Actuator. B Chem. 230, 184–190.
Martin, R.B., 1998. Biopolym. Orig. Res. Biomol. 45 (5), 351–353.
Mistry, K., Ibrahim, K.H., Novodchuk, I., Ngo, H.T., Imamura, G., Sanderson, J., Yavuz, M., Yoshikawa, G., Musselman, K.P., 2020. Adv. Mater. Technol. 5 (12), 2000704.
Morales, M.A., Halpern, J.M., 2018. Bioconjugate Chem. 29, 3231–3239.
Moudgil, A., Singh, S., Mishra, N., Mishra, P., Das, S., 2020. Adv. Mater. Technol. 5, 1–11.
Mu, L., Chang, Y., Sawtelle, S.D., Wipf, M., Duan, X., Reed, M.A., 2015. IEEE Access 3, 287–302.
Munief, W.M., Lu, X., Teucke, T., Wilhelm, J., Britz, A., Hempel, F., Lanche, R., Schwartz, M., Law, J.K.Y., Grandthyll, S., Müller, F., Neurohr, J.U., Jacobs, K., Schmitt, M., Pachauri, V., Hempelmann, R., Ingebrandt, S., 2019. Biosens. Bioelectron. 126, 136–142.
Novodchuk, I., Bajcsy, M., Yavuz, M., 2020. Carbon N. Y. 172, 431–453.
Novodchuk, I., Irannejad, M., Wales, B., Ibrahim, K., Sanderson, J., Bajcsy, M., Yavuz, M., 2019a. Mater. Res. Bull. 111.
Novodchuk, I., Kayaharman, M., Ibrahim, K., Al-Tuairqi, S., Irannejad, M., Abdel-Rahman, E., Sanderson, J., Bajcsy, M., Yavuz, M., 2020. B/N co-doped graphene oxide gel with extremely-high mobility and ION/IOFF for large-area field effect transistors. Carbon 158, 624–630.
Piccinini, E., Alberti, S., Longo, G.S., Berninger, T., Breu, J., Dostalek, J., Azzaroni, O., Knoll, W., 2018. J. Phys. Chem. C 122, 10181–10188.
Ramadhan, A., Wesolowski, M., Wakabayashi, T., Shiromaru, H., Fujino, T., Kodama, T., Duley, W., Sanderson, J., 2017. Carbon N. Y. 118, 680–685.
Roberts, A., Cormode, D., Reynolds, C., Newhouse-Illige, T., LeRoy, B.J., Sandhu, A.S., 2011. Appl. Phys. Lett. 99 (5), 051912.
Sarangadharan, I., Hsu, C.-P., Chu, C.-H., Regmi, A., Chen, Y.W., Wang, Y.-L., 2017. ECS Trans 77, 11–15.
Sarangadharan, I., Huang, S.W., Kuo, W.C., Chen, P.H., Wang, Y.L., 2019. Sensor. Actuator. B Chem. 285, 209–215.
Sarangadharan, I., Wang, S.L., Tai, T.Y., Pulikkathodi, A.K., Hsu, C.P., Chiang, H.H.K., Liu, L.Y.M., Wang, Y.L., 2018. Biosens. Bioelectron. 107, 259–265.
Seo, G., Lee, G., Kim, M.J., Baek, S.H., Choi, M., Ku, K.B., Lee, C.S., Jun, S., Park, D., Kim, H.G., Kim, S.J., Lee, J.O., Kim, B.T., Park, E.C., Kim, S. Il, 2020. ACS Nano 14, 5135–5142.
Šindler-Kulyk, M., Tomšić, S., Marinić, Ž., Metelko, B., 1995. Recl. des Trav. Chim. des Pays-Bas 114 (11-12), 476–479.
Sinha, A., Tai, T.Y., Li, K.H., Gopinathan, P., Chung, Y. Da, Sarangadharan, I., Ma, H.P., Huang, P.C., Shiesh, S.C., Wang, Y.L., Lee, G. Bin, 2019. Biosens. Bioelectron. 129, 155–163.
Stolyarov, M.A., Liu, G., Rumyantsev, S.L., Shur, M., Balandin, A.A., 2015. Appl. Phys. Lett. 107, 28–33.
Su, Y., Cao, S., Shi, L.B., Qian, P., 2020. Appl. Surf. Sci. 531, 14734.
Welch, N.G., Scoble, J.A., Muir, B.W., Pigram, P.J., 2017. Biointerphases 12, 02D301.